Wenhao Shen
State Key Laboratory of Nonlinear Mechanics (LNM),
Institute of Mechanics,
Chinese Academy of Sciences,
Beijing 100190, China;
School of Engineering Science,
University of Chinese Academy of Sciences,
Beijing 100049, China

Ya-Pu Zhao[1]
State Key Laboratory of Nonlinear Mechanics (LNM),
Institute of Mechanics,
Chinese Academy of Sciences,
Beijing 100190, China;
School of Engineering Science,
University of Chinese Academy of Sciences,
Beijing 100049, China
e-mail: yzhao@imech.ac.cn

Quasi-Static Crack Growth Under Symmetrical Loads in Hydraulic Fracturing

Symmetrical load on the crack surfaces is found in many fluid–solid problems. The combined effect of symmetrical normal and shear stresses is investigated, which impacts on the displacement and stress fields and the predictions of crack initiation and deflection. The boundary integral equations of displacement and stress fields are formulated using the integral-transform method. The equations of the displacement and stress are reduced using the Abel integral equations. The analytical solution of the full space for uniform normal and shear stresses is obtained. The asymptotic solution of the displacement of the crack surface is obtained near the crack tip under specific normal and shear stresses. Results show that shear stress tends to inhibit the crack, and the predictions of crack initiation and deflection could be inappropriate for a slit crack under a singular shear stress. This study may be useful for future investigations of the fluid–solid problems and help to understand the hydraulic fracturing. [DOI: 10.1115/1.4036988]

Keywords: hydraulic fracturing, shear stress, symmetrical load, crack initiation, crack deflection

1 Introduction

Cracks under symmetrical load on the crack surfaces have been found in many fluid–solid interaction problems, such as magma- or water-driven cracks in the earth's crust or glacier beds [1,2], the stimulation of hydrocarbon-bearing rock strata to enhance the production of oil and gas wells [3,4], and the fabrication of flexible structures and electronics [5], etc. Cracks are driven by both normal and shear stresses, which are of certain distributions and symmetrical about crack center (see Fig. 1) so that shear stress is zero in front of the crack tip. Thus, there is only mode I crack in this problem.

The predictions of crack initiation [6–8] and deflection [9] require the asymptotic solutions of displacement and stress fields [10,11]. A non-square-root singularity of the stress field at the crack tip [1–4,12,13] has been reported in hydraulic fracturing. A viscous fluid was injected at the crack center forcing the crack to be fractured straightly and continuously. There is a strong coupling between the incompressible viscous fluid flow and the crack propagation. Non-square-root singularities of the hydrodynamic pressure in the crack and stress field in the solid emerge. To address the incompatibility of singularities, a dry zone or a fluid lag, in which there is no viscous fluid, was introduced near the crack tip. Using the fluid-lag model, the normal stress yields the square-root singularity, and the hydrodynamic pressure has no singularity. The fluid lag is known to exist physically [3]. However, the fluid lag has been neglected in many studies, and whether the effect of fluid lag is negligible or not still remains unsolved [14–16]. If the fluid lag is neglected as the assumption of most work [1–4,13], the non-square-root stress singularity in the solid resurfaces. This non-square-root singularity is due to the normalization process where the dimensionless stress intensity factor (SIF) is very small, and has been set to zero in most of the previous studies [1–3]. The shear stress on the crack surfaces was considered negligible in the previous studies. There has been a brief discussion [4] on the singularity issue under the singular symmetrical normal and shear stresses on the crack surfaces. In this study, we focus on the formulation of symmetrical load on the crack surface with different approaches, and the predictions of crack initiation and deflection. No fluid lag is assumed, and the normal and shear stresses are assumed to be power-law functions of the distance from crack tip.

This study aims to investigate the combined effect of symmetrical normal and shear stresses on the displacement and stress fields, the criteria of initiation and the prediction of deflection of a slit crack. Using the integral-transform method [5,10,17] and based on the linear elastic fracture mechanics (LEFM), the boundary integral equations of displacement and stress fields are derived, and the analytical solution for uniform normal and shear stresses is obtained. Based on three subproblems from hydraulic fracturing, the strain energy release rate (SERR) and the SIF are calculated and discussed for uniform and power-law symmetrical normal and shear stresses using the reversible thermodynamic crack cycle. The applicability of three typical prediction methods of crack deflection is discussed.

2 Mathematical Formulation

There is only a Griffith-type crack of length l in the linear-elastic full space, as shown in Fig. 1. Cartesian coordinate system is used such that the origin coincides with the crack center, and the x_1-axis and x_2-axis are parallel and perpendicular to the crack plane, respectively. The crack is in plane strain state. For convenience and without loss of generality, we focus on the first quadrant where $x_1 > 0$ and $x_2 > 0$. Hooke's law gives the relationship between stress tensor, $\boldsymbol{\sigma}$, and infinitesimal strain tensor, $\boldsymbol{\gamma}$, as

$$\boldsymbol{\sigma} = \lambda\gamma\mathbf{I} + 2\mu\boldsymbol{\gamma} \quad \text{with} \quad \boldsymbol{\gamma} = (\nabla\boldsymbol{u} + \boldsymbol{u}\nabla)/2 \tag{1}$$

where $\gamma = \mathrm{tr}(\boldsymbol{\gamma})$ is the dilatation of an infinitesimal element, λ and μ are the Lamé coefficients, and $\mathbf{I}$ is the second-rank identity

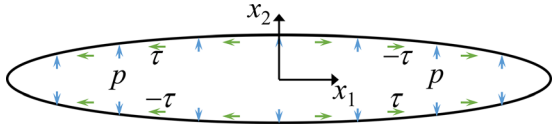

Fig. 1 Schematic diagram of symmetrical normal and shear stresses on a slit crack. The stresses are symmetrical about both the coordinate axes.

[1]Corresponding author.

Contributed by the Applied Mechanics Division of ASME for publication in the JOURNAL OF APPLIED MECHANICS. Manuscript received March 12, 2017; final manuscript received June 4, 2017; published online June 20, 2017. Assoc. Editor: Thomas Siegmund.

tensor. The inertial effect is neglected for the quasi-static crack growth. The equations of equilibrium are [5,17]

$$\nabla^2 \boldsymbol{u} + \frac{1}{1-2\nu}\nabla\gamma = 0 \tag{2}$$

$$\nabla^2 \gamma = 0 \tag{3}$$

where ν is the Poisson's ratio. There are arbitrary symmetrical normal and shear stresses acting on the crack surfaces. The dynamic conditions on the crack surface are

$$\sigma_{22}(x_1, 0^+) = -p(x_1), \quad x_1 \in (0, l) \tag{4}$$

$$\sigma_{12}(x_1, 0^+) = \tau(x_1), \quad x_1 \in (0, l) \tag{5}$$

Due to the symmetry of geometry and load, the displacement and stress fields are symmetrical about the x_1-axis, and the displacement and stress components, which are skew-symmetrical about the x_1-axis, are zero. There are

$$u_2(x_1, 0^+) = 0, \quad x_1 \in (l, \infty) \tag{6}$$

$$\sigma_{12}(x_1, 0^+) = 0, \quad x_1 \in (l, \infty) \tag{7}$$

Assuming that there are no tractions at infinity, the stress and displacement decrease to zero. Furthermore, the contribution of the tractions at infinity can be taken into consideration by superposition due to the linear elastic assumption.

3 Solution to the Crack Problem

Fourier transforms are used to solve Eqs. (2) and (3) subjected to boundary conditions (4)–(7). The solution of transformed equations is expressed with two auxiliary functions. The inverse Fourier transforms of displacement and stress are reduced with Abel integral equations [18].

3.1 Preliminary Results: the Auxiliary Functions. The Fourier sine and cosine transforms, $\mathcal{F}_s\{*\}$ and $\mathcal{F}_c\{*\}$, of semi-infinite space can be expressed as

$$\mathcal{F}_s\{*\} = \sqrt{\frac{2}{\pi}}\int_0^\infty * \sin(kx)\mathrm{d}x \quad \text{and} \quad \mathcal{F}_c\{*\} = \sqrt{\frac{2}{\pi}}\int_0^\infty * \cos(kx)\mathrm{d}x \tag{8}$$

of which the inverse Fourier sine and cosine transforms, $\mathcal{F}_s^{-1}\{*\}$ and $\mathcal{F}_c^{-1}\{*\}$, are

$$\mathcal{F}_s^{-1}\{*\} = \sqrt{\frac{2}{\pi}}\int_0^\infty * \sin(kx)\mathrm{d}k \quad \text{and} \quad \mathcal{F}_c^{-1}\{*\} = \sqrt{\frac{2}{\pi}}\int_0^\infty * \cos(kx)\mathrm{d}k \tag{9}$$

Denote the Fourier transforms of the displacement vector, $\boldsymbol{u}$, and the dilatation, γ, as $\boldsymbol{U}$, and Ξ, respectively. u_1 is an odd function, the Fourier sine transform is used. Similarly, Fourier cosine transform is used for u_2 and γ. The use of Fourier transform reduces Eqs. (2) and (3) to a set of ordinary differential equations, of which the solutions are

$$\begin{cases} U_1 = \dfrac{1}{k}\left[kB + \dfrac{(3-4\nu)A}{2(1-2\nu)} - \dfrac{kAx_2}{2(1-2\nu)}\right]\mathrm{e}^{-kx_2} \\ U_2 = \left[B - \dfrac{Ax_2}{2(1-2\nu)}\right]\mathrm{e}^{-kx_2} \end{cases} \quad \text{and } \Xi = A\mathrm{e}^{-kx_2} \tag{10}$$

where $A(x_1, k)$ and $B(x_1, k)$ are unknown functions to be determined from the boundary conditions. Using the inverse Fourier transforms of the stress and displacement components, one obtains

$$\sigma_{11} = \mu\mathcal{F}_c^{-1}\left\{\left[2kB + \frac{3-2\nu}{1-2\nu}A - \frac{kAx_2}{1-2\nu}\right]\mathrm{e}^{-kx_2}\right\} \tag{11}$$

$$\sigma_{22} = -\mu\mathcal{F}_c^{-1}\left\{\left(A - \frac{kAx_2}{1-2\nu} + 2kB\right)\mathrm{e}^{-kx_2}\right\} \tag{12}$$

$$\sigma_{12} = -2\mu\mathcal{F}_s^{-1}\left\{\left[\frac{1-\nu}{1-2\nu}A - \frac{kAx_2}{2(1-2\nu)} + kB\right]\mathrm{e}^{-kx_2}\right\} \tag{13}$$

$$u_1 = \mathcal{F}_s^{-1}\left\{\frac{1}{k}\left[kB + \frac{(3-4\nu)A}{2(1-2\nu)} - \frac{kAx_2}{2(1-2\nu)}\right]\mathrm{e}^{-kx_2}\right\} \tag{14}$$

$$u_2 = \mathcal{F}_c^{-1}\left\{\left[B - \frac{Ax_2}{2(1-2\nu)}\right]\mathrm{e}^{-kx_2}\right\} \tag{15}$$

Substituting Eqs. (12), (13), and (15) into the boundary conditions (4)–(7) yields a set of integral equations of $A(x_1, k)$ and $B(x_1, k)$ as

$$\mu\mathcal{F}_c^{-1}\{A + 2kB\} = p(x_1), \quad \text{for } x_1 \in (0, l) \tag{16}$$

$$\mathcal{F}_c^{-1}\{B\} = 0, \quad \text{for } x_1 \in (l, \infty) \tag{17}$$

$$-2\mu\mathcal{F}_s^{-1}\left\{\frac{1-\nu}{1-2\nu}A + kB\right\} = \tau(x_1), \quad \text{for } x_1 \in (0, l) \tag{18}$$

$$\mathcal{F}_s^{-1}\left\{\frac{1-\nu}{1-2\nu}A + kB\right\} = 0, \quad \text{for } x_1 \in (l, \infty) \tag{19}$$

Following the approach given by Sneddon and Lowengrub [10], the functions of $A(x_1, k)$ and $B(x_1, k)$ can be determined from two auxiliary functions of $\varphi(t)$ and $\psi(t)$ as

$$B = \int_0^l \varphi(t)J_0(kt)\mathrm{d}t \quad \text{and} \quad \frac{1-\nu}{(1-2\nu)k}A + B = \int_0^l \psi(t)J_0(kt)\mathrm{d}t \tag{20}$$

which satisfy Eqs. (17) and (19), according to the following identities:

$$\int_0^\infty J_0(kt)\sin(kx)\mathrm{d}k = \frac{\mathbb{H}(x-t)}{\sqrt{x^2-t^2}} \quad \text{and} \quad \int_0^\infty J_0(kt)\cos(kx)\mathrm{d}k = \frac{\mathbb{H}(t-x)}{\sqrt{t^2-x^2}} \tag{21}$$

Here, $\mathbb{H}(*)$ is the Heaviside function. The solutions of the auxiliary functions are

$$\varphi(t) = \frac{(1-\nu)t}{\mu}\sqrt{\frac{2}{\pi}}\int_0^t \frac{\Delta p(s)\mathrm{d}s}{\sqrt{t^2-s^2}} + \frac{(1-2\nu)t}{2\mu}\sqrt{\frac{2}{\pi}}\int_t^l \frac{\tau(s)\mathrm{d}s}{\sqrt{s^2-t^2}} \tag{22}$$

$$\psi(t) = -\frac{t}{2\mu}\sqrt{\frac{2}{\pi}}\int_t^l \frac{\tau(s)\mathrm{d}s}{\sqrt{s^2-t^2}} \tag{23}$$

The detailed derivation of Eqs. (22) and (23) is given in Appendix A.

3.2 Displacement Field. Substituting the equations of auxiliary functions (22) and (23) into the inverse Fourier transforms of the displacement components, Eqs. (14) and (15), there are

$$u_1(x_1,x_2) = -\frac{4}{\pi E'}\mathrm{Im}\left[\frac{1-2\nu}{2(1-\nu)}I_\mathrm{P} + I_\mathrm{T}\right] - \frac{2x_2}{\pi E'(1-\nu)}\frac{\partial}{\partial x_1}\mathrm{Re}(I_\mathrm{P}+I_\mathrm{T}) \tag{24}$$

$$u_2(x_1,x_2) = \frac{4}{\pi E'}\mathrm{Re}\left[I_\mathrm{P} + \frac{1-2\nu}{2(1-\nu)}I_\mathrm{T}\right] + \frac{2x_2}{\pi E'(1-\nu)}\frac{\partial}{\partial x_1}\mathrm{Im}(I_\mathrm{P}+I_\mathrm{T}) \tag{25}$$

where Re and Im represent the real and imaginary parts of a complex number, respectively, $E' = E/(1-\nu^2)$ with E being Young's modulus, and

$$I_\mathrm{P}(x_1,x_2) = \int_0^l \frac{t\mathrm{d}t}{\sqrt{t^2+x_2^2-x_1^2-\mathrm{i}2x_1x_2}}\int_0^t \frac{p(s)\mathrm{d}s}{\sqrt{t^2-s^2}} \tag{26}$$

$$I_\mathrm{T}(x_1,x_2) = \int_0^l \frac{t\mathrm{d}t}{\sqrt{t^2+x_2^2-x_1^2-\mathrm{i}2x_1x_2}}\int_t^l \frac{\tau(s)\mathrm{d}s}{\sqrt{s^2-t^2}} \tag{27}$$

See Appendix B for the detailed derivation. Even though these iterated integrals have advantages in finding analytical solutions for uniform normal and shear stresses, these are not easy to be numerically calculated. Single integrals of reduced form are obtained by changing the order of the integrations as

$$u_1(x_1,x_2) = -\frac{4}{\pi E'}\mathrm{Im}\left[\frac{1-2\nu}{2(1-\nu)}Z_{\mathrm{P},0} + Z_{\mathrm{T},0}\right] - \frac{2x_2}{\pi E'(1-\nu)}\mathrm{Re}(Z_{\mathrm{T},1}+Z_{\mathrm{P},1}) \tag{28}$$

$$u_2(x_1,x_2) = \frac{4}{\pi E'}\mathrm{Re}\left[Z_{\mathrm{P},0} + \frac{1-2\nu}{2(1-\nu)}Z_{\mathrm{T},0}\right] + \frac{2x_2}{\pi E'(1-\nu)}\mathrm{Im}(Z_{\mathrm{P},1}+Z_{\mathrm{T},1}) \tag{29}$$

in which the variables $Z_{\mathrm{P},k}$ and $Z_{\mathrm{T},k}$ are defined by

$$Z_{\mathrm{P},k}(x_1,x_2) = \frac{\partial^k}{\partial x_1^k}\int_0^l p(s)K_\mathrm{P}(s;x_1,x_2)\mathrm{d}s \tag{30}$$

$$Z_{\mathrm{T},k}(x_1,x_2) = \frac{\partial^k}{\partial x_1^k}\int_0^l \tau(s)K_\mathrm{T}(s;x_1,x_2)\mathrm{d}s \tag{31}$$

where the kernel functions $K_\mathrm{P}(s;x_1,x_2)$ and $K_\mathrm{T}(s;x_1,x_2)$ are

$$K_\mathrm{P}(s;x_1,x_2) = \ln\frac{\sqrt{1-s^2}+\sqrt{1-(x_1+\mathrm{i}x_2)^2}}{\sqrt{s^2-(x_1+\mathrm{i}x_2)^2}} \tag{32}$$

$$K_\mathrm{T}(s;x_1,x_2) = \frac{\pi}{2} + \mathrm{i}\tanh^{-1}\frac{x_1+\mathrm{i}x_2}{s} \tag{33}$$

Note that $K_\mathrm{P}(s;x_1,x_2)$ and $K_\mathrm{T}(s;x_1,x_2)$ are derived with $x_2>0$ in the first quadrant, i.e., Eqs. (32) and (33) may be inappropriate to get the solution for $x_2=0$. The inapplicability is due to $\mathrm{Im}K_\mathrm{P}$ changing its sign from $x_2\to 0^+$ to $x_2=0$. The solutions for the rest three quadrants can be obtained with the symmetry.

For $x_2=0^+$ in the first quadrant, using Eqs. (24) and (25), the displacement components of the crack surface are found to be

$$u_1(x_1,0^+) = \begin{cases} \dfrac{4}{\pi E'}\displaystyle\int_0^{x_1}\frac{t\mathrm{d}t}{\sqrt{x_1^2-t^2}}\left[-\frac{1-2\nu}{2(1-\nu)}\int_0^t\frac{p(s)\mathrm{d}s}{\sqrt{t^2-s^2}} - \int_t^l\frac{\tau(s)\mathrm{d}s}{\sqrt{s^2-t^2}}\right], & x_1\in(0,l) \\ \dfrac{4}{\pi E'}\displaystyle\int_0^{l}\frac{t\mathrm{d}t}{\sqrt{x_1^2-t^2}}\left[-\frac{1-2\nu}{2(1-\nu)}\int_0^t\frac{p(s)\mathrm{d}s}{\sqrt{t^2-s^2}} - \int_t^l\frac{\tau(s)\mathrm{d}s}{\sqrt{s^2-t^2}}\right], & x_1\in(l,\infty) \end{cases} \tag{34}$$

$$u_2(x_1,0^+) = \begin{cases} \dfrac{4}{\pi E'}\displaystyle\int_{x_1}^l\frac{t\mathrm{d}t}{\sqrt{t^2-x_1^2}}\left[\int_0^t\frac{p(s)\mathrm{d}s}{\sqrt{t^2-s^2}} + \frac{1-2\nu}{2(1-\nu)}\int_t^l\frac{\tau(s)\mathrm{d}s}{\sqrt{s^2-t^2}}\right], & x_1\in(0,l) \\ 0, & x_1\in(l,\infty) \end{cases} \tag{35}$$

The displacement of the crack surface depends on both the normal and the shear stresses. Equation (35) reduces to the result of the crack opening under the action of normal stress only [10], for the contribution of the shear stress being negligible. Exchanging the order of the integrations in Eqs. (34) and (35) yields

$$u_1(x_1,0^+) = \begin{cases} -\dfrac{1-2\nu}{(1-\nu)E'}\displaystyle\int_0^{x_1}p(s)\mathrm{d}s - \frac{4}{\pi E'}\int_0^l\tau(s)\ln\sqrt{\left|\frac{x_1+s}{x_1-s}\right|}\mathrm{d}s, & x_1\in(0,l) \\ -\dfrac{2(1-2\nu)}{\pi E'(1-\nu)}\displaystyle\int_0^l p(s)\left(\frac{\pi}{2}-\arctan\frac{\sqrt{x_1^2-l^2}}{\sqrt{l^2-s^2}}\right)\mathrm{d}s - \frac{4}{\pi E'}\int_0^l\tau(s)\ln\sqrt{\left|\frac{x_1+s}{x_1-s}\right|}\mathrm{d}s, & x_1\in(l,\infty) \end{cases} \tag{36}$$

$$u_2(x_1,0^+) = \begin{cases} \dfrac{4}{\pi E'}\displaystyle\int_0^l p(s)\ln\frac{\sqrt{l^2-x_1^2}+\sqrt{l^2-s^2}}{\sqrt{|x_1^2-s^2|}}\mathrm{d}s + \frac{1-2\nu}{(1-\nu)E'}\int_{x_1}^l\tau(s)\mathrm{d}s, & x_1\in(0,l) \\ 0, & x\in(l,\infty) \end{cases} \tag{37}$$

Note that Eqs. (28), (29), (36), and (37) are not Cauchy principal value integrals, and can be numerically calculated readily. However, Eqs. (24), (25), (34), and (35) are suggested when analytical solution is needed.

3.3 Stress Field. Similarly, substituting the auxiliary functions (22) and (23) into the inverse Fourier transforms of the components of stress, Eqs. (11)–(13), the components of stress tensor can be obtained as

$$\sigma_{11}(x_1,x_2) = -\frac{2}{\pi}\frac{\partial}{\partial x_1}\mathrm{Im}(I_\mathrm{P}+2I_\mathrm{T}) - \frac{2x_2}{\pi}\frac{\partial^2}{\partial x_1^2}\mathrm{Re}(I_\mathrm{P}+I_\mathrm{T}) \quad (38)$$

$$\sigma_{22}(x_1,x_2) = -\frac{2}{\pi}\frac{\partial}{\partial x_1}\mathrm{Im}I_\mathrm{P} + \frac{2x_2}{\pi}\frac{\partial^2}{\partial x_1^2}\mathrm{Re}(I_\mathrm{P}+I_\mathrm{T}) \quad (39)$$

$$\sigma_{12}(x_1,x_2) = -\frac{2}{\pi}\frac{\partial}{\partial x_1}\mathrm{Re}I_\mathrm{T} + \frac{2x_2}{\pi}\frac{\partial^2}{\partial x_1^2}\mathrm{Im}(I_\mathrm{P}+I_\mathrm{T}) \quad (40)$$

Exchanging the order of the integrations, one obtains the single integrals of stress components as

$$\sigma_{11}(x_1,x_2) = -\frac{2}{\pi}\mathrm{Im}(Z_{\mathrm{P},1}+2Z_{\mathrm{T},1}) - \frac{2x_2}{\pi}\mathrm{Re}(Z_{\mathrm{P},2}+Z_{\mathrm{T},2}) \quad (41)$$

$$\sigma_{22}(x_1,0^+) = -\frac{2}{\pi}\mathrm{Im}Z_{\mathrm{P},1} + \frac{2x_2}{\pi}\mathrm{Re}(Z_{\mathrm{P},2}+Z_{\mathrm{T},2}) \quad (42)$$

$$\sigma_{12}(x_1,x_2) = -\frac{2}{\pi}\mathrm{Re}Z_{\mathrm{T},1} + \frac{2x_2}{\pi}\mathrm{Im}(Z_{\mathrm{P},2}+Z_{\mathrm{T},2}) \quad (43)$$

Using Eqs. (38)–(40), the expressions of stress components at $x_2 = 0^+$ degenerate to

$$\sigma_{11}(x_1,0^+) = \begin{cases} -p(x_1) + \dfrac{4}{\pi}\displaystyle\int_0^l \frac{\tau(s)s\mathrm{d}s}{x_1^2-s^2}, & x_1 \in (0,l) \\ \dfrac{2}{\pi}\dfrac{x_1}{\sqrt{x_1^2-l^2}}\displaystyle\int_0^l p(s)\frac{\sqrt{l^2-s^2}}{x_1^2-s^2}\mathrm{d}s + \frac{4}{\pi}\int_0^l \frac{\tau(s)s\mathrm{d}s}{x_1^2-s^2}, & x_1 \in (l,\infty) \end{cases} \quad (44)$$

$$\sigma_{22}(x_1,0^+) = \begin{cases} -p(x_1), & x_1 \in (0,l) \\ \dfrac{2}{\pi}\dfrac{x_1}{\sqrt{x_1^2-l^2}}\displaystyle\int_0^l p(s)\frac{\sqrt{l^2-s^2}}{x_1^2-s^2}\mathrm{d}s, & x_1 \in (l,\infty) \end{cases} \quad (45)$$

$$\sigma_{12}(x_1,0^+) = \begin{cases} \tau(x_1) & x_1 \in (0,l) \\ 0, & x_1 \in (l,\infty) \end{cases} \quad (46)$$

Note that the second term on the right-hand side of Eq. (44) is a Cauchy principal value integral for $x_1 \in (0,l)$. The singularity of Cauchy principal value integral can be removed by putting a derivative with respect to x_1 outside the integral. The stress components in front of the crack tip are used to calculate the SIF and the SERR.

3.4 Strain Energy Release Rate (SERR) and Stress Intensity Factor (SIF). The method of reversible thermodynamic recycle [19,20] is adopted to calculate the SERR. The method treats the role of surface energy as a traction on the surface [19]. The mechanical energy decrement equals to the work done by the traction on the crack surfaces, $E_\mathrm{M} = -W_\mathrm{t}$. Thus, the calculation of decrement of mechanical energy does not require any information of the external forces and the total strain energy. The work done by the traction is

$$W_\mathrm{t} = -4\int_0^{\Delta l}\frac{1}{2}\left[\sigma_{22}(l+s,0^+)u_2(l+s,0^+) + \sigma_{12}(l+s,0^+)u_1(l+s,0^+)\right]\mathrm{d}s \quad (47)$$

in which the coefficient, 4, is due to the use of a quarter of the crack surface, and 1/2 is due to the linear relationship between stress and displacement. σ_{11} is not included because it acts on the $x_1 - x_3$ plane, which is perpendicular to crack surface. A symmetrical stress has no influence on σ_{22} and σ_{12} such that $\sigma_{12} = 0$. The traction equals to σ_{22} in front of the crack tip. The SERR is calculated as

$$G = -\frac{\mathrm{d}E_\mathrm{M}}{\mathrm{d}l} = \lim_{\Delta l\to 0^+}\frac{2}{\Delta l}\int_0^{\Delta l}\sigma_{22}(l+s,0^+)u_2(l+s,0^+)\mathrm{d}s \quad (48)$$

where σ_{22} is the stress component with the crack length being l and u_2 is the displacement with the crack length being $l+\Delta l$.

From the equations of stress components, the SIF of mode **I** crack is used to be calculated using $K_\mathrm{I} = \lim_{x_1\to l^+}\sqrt{2\pi(x_1-l)}\sigma_{22}$. Note that the shear stress has no explicit effect on the SIF according to Eq. (45). However, a shear stress on the crack surface leads to an increment of displacement according to Eqs. (36) and (37). The use of the SIF to calculate the asymptotic solution of displacement near the crack tip, and vice versa, may be inappropriate in some circumstances [4]. The SIF reveals the square-root singularity of the stress field near the crack tip [7], and there is $\sigma_{11} = K_1/\sqrt{2\pi(x_1-l)}$ in front of the crack tip. Considering the important role of shear stress, σ_{11} is used in this study to calculate the SIF as

$$K_\mathrm{I} = \lim_{x_1\to l^+}\sqrt{2\pi(x_1-l)}\sigma_{11} \quad (49)$$

in which, σ_{11} consists of σ_{22} and an additional shear-stress term on the right-hand side of Eq. (44) for $x_1 \in (l,\infty)$. In Sec. 4, Eq. (49) is used for the validation of $K_\mathrm{I} = \lim_{x_1\to l^+}\sqrt{2\pi(x_1-l)}\sigma_{22}$, which has long been used.

4 Quasi-Static Crack Growth Under Specific Loads

In the modeling of hydraulic fracturing, singular normal and shear stresses have been reported [1–4,12,13]. Under the assumption of inviscid fracturing fluid, the normal stress (pressure) remains uniform along the crack, and no shear stress acts on the crack surfaces. Using the Newtonian fracturing fluid and lubrication approximation, there is competition among elasticity, fluid viscosity, and fracture toughness. The lubrication approximation may be inappropriate near the crack tip. However, its effect on the average of the displacement of the crack surface is negligible [4]. The competition results in multiple length scales and different asymptotes that depend on the distance from the crack tip. Thus, two regions that are viscosity-dominant and toughness-dominant emerge. The sizes of the regions are controlled by one dimensionless parameter, which represents the ratio of toughness to viscosity [3]. If an extremely large toughness is assumed, the viscosity-dominant region vanishes, the singularity of normal stresses is characterized as $\ln(l-x_1)$, and the asymptotic solution of crack opening, which is two times of u_2 of crack surface, is $O[(l-x_1)^{1/2}]$ [3,4]. If an extremely large viscosity is assumed, there are $p \sim -(l-x_1)^{-1/3}$ and $u_2 \sim (l-x_1)^{2/3}$. According to the lubrication approximation, the shear stress is related to crack opening and the gradient of normal stress as $\tau = u_2(x_1,0^+)\partial p/\partial x_1$. The singularities of shear stress are characterized as $-(l-x_1)^{-1/2}$ and $-(l-x_1)^{-2/3}$ for problems with extremely large toughness and extremely large viscosity, respectively. The dimensionless fracture toughness is finite and positive in the toughness-dominant problems and zero in the viscosity-dominant problems. Thus, three subproblems are proposed as

(1) $\tilde{p}(\tilde{x}_1)=1, \tilde{\tau}(\tilde{x}_1)=0$

(2) $\tilde{p}(\tilde{x}_1)=1+\ln 4+\ln(1-\tilde{x}_1^2), \tilde{\tau}(\tilde{x}_1)=-(1-\tilde{x}_1^2)^{-1/2}$

(3) $\tilde{p}(\tilde{x}_1)=\Gamma(1/6)/\sqrt{\pi}\Gamma(2/3)-(1-\tilde{x}_1^2)^{-1/3}, \tilde{\tau}(\tilde{x}_1)=-(1-\tilde{x}_1^2)^{-2/3}$

where $(\tilde{p},\tilde{\tau})=2(p,\tau)/E'$, $(\tilde{x}_1,\tilde{x}_2,\tilde{u}_1,\tilde{u}_2)=(x_1,x_2,u_1,u_2)/l$, and $\Gamma(*)$ is the Gamma function. It should be noted that the expressions of $\tilde{p}$ and $\tilde{\tau}$ are from the coupling of lubrication and elasticity equations, and the coupling neglects the effect of shear stress, i.e., $\tilde{p}$ is from the full coupling of lubrication and elasticity equations with the absence of shear stress and $\tilde{\tau}$ is from the equilibrium equation. The coupling of $\tilde{\tau}$ is one-way. The constants of $\tilde{p}(\tilde{x}_1)$ are used to set the dimensionless SIF, $\tilde{K}_I=2K_I/E'\sqrt{\pi l}$, to 1, 1 and 0, respectively. Subproblems (1)–(3) are related to problems with nonviscid fluid, large fracture toughness, and large viscosity, respectively. It should be noticed that K_I in this paragraph is calculated with $K_I=\lim_{x_1\to l^+}\sqrt{2\pi(x_1-l)}\sigma_{22}$. Note that the discussion of singularity issue is focusing on the power-law exponents of normal and shear stresses, and is irrelevant with the average values of the loads.

4.1 Analytical Solution for Uniform p and τ. There is analytical solution to the first subproblem. Focus on a general case where $\tilde{p}$ and $\tilde{\tau}$ are constant. It is difficult to do the iterated integral, I_T, of Eq. (27). The analytical solution for full space can be obtained by integrating I_P and $Z_{T,0}$, which are

$$I_P=\frac{\pi\tilde{p}(\tilde{x}_2-i\tilde{x}_1)}{2}\left[\sqrt{1+\frac{1}{(\tilde{x}_2-i\tilde{x}_1)^2}}-1\right] \tag{50}$$

$$Z_{T,0}=i\tilde{\tau}\left\{\coth^{-1}(\tilde{x}_1+i\tilde{x}_2)+\frac{1}{2}(\tilde{x}_1+i\tilde{x}_2)\ln\left[1+\frac{1}{(\tilde{x}_2-i\tilde{x}_1)^2}\right]\right\} \tag{51}$$

Both I_P and $Z_{T,0}$ are applicable for $x_2=0$ except for two singular points, (0, 0) and (1, 0). The analytical solutions of the displacement and stress fields in full space are in Appendix C.

According to the first term in Eq. (35) and second term in Eq. (37), the analytical solution of displacement component at the crack surface is

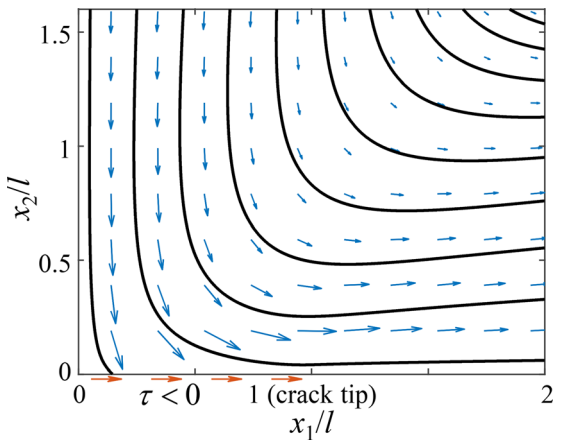

Fig. 2 Normalized displacement of the solid in the first quadrant. A uniform and negative shear stress acts on the crack surface. Arrows represent displacement vectors. Solid lines are tangent to the displacement.

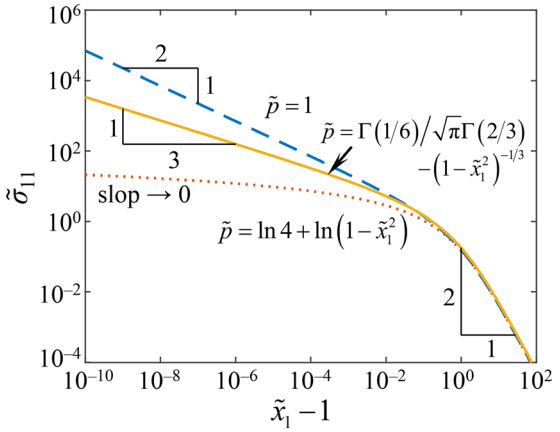

Fig. 3 Dimensionless stress component, $\tilde{\sigma}_{11}$, in front of the crack tip under different normal stresses ($\tilde{x}_2=0^+$)

$$\tilde{u}_2(\tilde{x}_1,0^+)=\tilde{p}\sqrt{1-\tilde{x}_1^2}+\frac{(1-2\nu)\tilde{\tau}}{2(1-\nu)}(1-\tilde{x}_1),\quad \tilde{x}_1\in(0,1) \tag{52}$$

which refers to half of the "crack opening" in hydraulic fracturing [3]. Crack opening is a linear function of the shear stress, and the derivative of the crack opening with respect to x_1 is discontinuous at the crack center. A negative shear stress will inhibit the opening of the crack. Due to symmetry, a uniform and negative shear stress acting on a slit crack results in $u_2=0$ in front of the crack tip and $u_1=0$ along the x_2-axis in the first quadrant. Figure 2 shows normalized displacement vectors and their tangential curves. The negative shear stress leads to a counterclockwise rotation which introduces negative u_2 near the crack surface. Such behavior will likely result in the crack closure.

The dimensionless stress components, $\tilde{\sigma}_{11}$ and $\tilde{\sigma}_{22}$, on the crack plane in front of the crack tip, according to Eqs. (44) and (45), are

$$\tilde{\sigma}_{11}(\tilde{x}_1,0^+)=\tilde{p}\left(\frac{\tilde{x}_1}{\sqrt{\tilde{x}_1^2-1}}-1\right)+\frac{2\tilde{\tau}}{\pi}\ln\frac{\tilde{x}_1^2}{\tilde{x}_1^2-1},\quad \tilde{x}_1\in(1,\infty) \tag{53}$$

$$\tilde{\sigma}_{22}(\tilde{x}_1,0^+)=\tilde{p}\left(\frac{\tilde{x}_1}{\sqrt{\tilde{x}_1^2-1}}-1\right),\quad \tilde{x}_1\in(1,\infty) \tag{54}$$

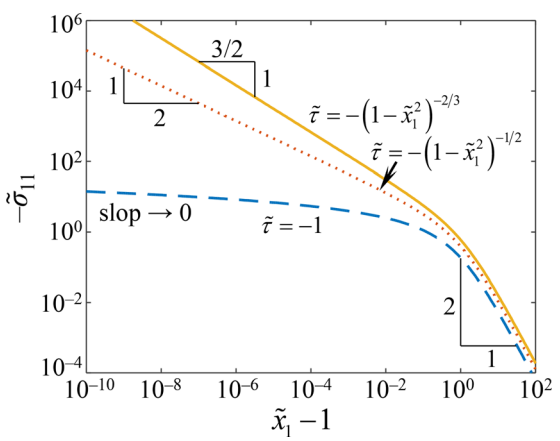

Fig. 4 Negative dimensionless stress component, $-\tilde{\sigma}_{11}$, in front of the crack tip under different shear stresses ($\tilde{x}_2=0^+$)

It is evident that a uniform normal stress leads to a square-root stress singularity at the crack tip and a uniform shear stress causes a logarithmic stress singularity.

4.2 Asymptotic Solutions Near the Crack Tip. Figures 3 and 4 plot the numerical solutions of dimensionless stress component, $\tilde{\sigma}_{11}$, in front of crack tip for normal-stress-only and shear-stress-only problems. According to Eqs. (44) and (45), $\tilde{\sigma}_{22}$ equals to $\tilde{\sigma}_{11}$ at $\tilde{x}_1 > 1$ and $\tilde{x}_2 = 0^+$. As a result, it is possible to replace $\tilde{\sigma}_{11}$ with $\tilde{\sigma}_{22}$ as the vertical axis of Fig. 3. In Fig. 3, the power-law exponent of the leading term of asymptotic solution is (1) $-1/2$ for a uniform normal stress of which the SIF is positive, (2) 0 for a normal stress with logarithmic singularity and the SIF being zero, and (3) $-1/3$ for a normal stress with its power-law exponent being $-1/3$ and the SIF being zero. The 2/1 power-law exponent shows that $\tilde{\sigma}_{11}$ has an inverse square asymptotic solution at infinity, which is in accord with Eq. (53) due to $\tilde{x}_1 \Big/ \sqrt{\tilde{x}_1^2 - 1} - 1 \sim \ln(\tilde{x}_1^2/\tilde{x}_1^2 - 1) \sim 1/\tilde{x}_1^2$ for $\tilde{x}_1 \to \infty$. A more general numerical solution reveals that for $\tilde{x}_1 \to 1^+$ there is

$$\tilde{\sigma}_{11}(\tilde{x}_1, 0^+) = \begin{cases} A_P(\tilde{x}_1^2 - 1)^{-1/2} + B_P(\tilde{x}_1^2 - 1)^{e_P} + O(1), & e_P \in (-1/2, 0) \\ A_P(\tilde{x}_1^2 - 1)^{-1/2} + B_P \ln(\tilde{x}_1^2 - 1) + O(1), & e_P = 0 \end{cases} \tag{55}$$

for a normal stress yielding $\tilde{p} = \tilde{p}_0 - (1 - \tilde{x}_1^2)^{e_P}$. The SIF becomes zero for $\tilde{p}_0 = \Gamma(1/2 + e_P)/\sqrt{\pi}\Gamma(1 + e_P)$. The constant A_P is related with the SIF as $A_P = \tilde{K}_I$, and B_P is a constant related to the distribution of the normal stress. In hydraulic fracturing, the crack length increases with time, which leads to the decreasing of $\tilde{K}_I$. The leading term of $\tilde{\sigma}_{11}$ changes from $A_P(\tilde{x}_1^2 - 1)^{-1/2}$ to $B_P(\tilde{x}_1^2 - 1)^{e_P}$ or $B_P \ln(\tilde{x}_1^2 - 1)$ for $\tilde{K}_I$ decreasing to zero. The asymptotic solution of displacement component, u_2, is given by

$$\tilde{u}_2(\tilde{x}_1, 0^+) = C_P\sqrt{1 - \tilde{x}_1^2} + D_P(1 - \tilde{x}_1^2)^{1+e_P} + O[(1 - \tilde{x}_1^2)^{3/2}], \quad e_P \in (-1/2, 1/2) \tag{56}$$

in which C_P and D_P are constants related to the normal stress, and $C_P = \tilde{K}_I$. For an arbitrary non-negative $\tilde{K}_I$, D_P is finite and positive.

A negative shear stress, $\tilde{\tau} = -(1 - \tilde{x}_1^2)^{e_T}$, results in a negative $\tilde{\sigma}_{11}$ according to Fig. 4. The power-law exponent of $\tilde{\sigma}_{11}$ increases with the distance from the crack tip and the increasing of e_T. According to a numerical calculation, the asymptotic solution of $\tilde{\sigma}_{11}$ for $\tilde{x}_1 \to 1^+$ due to a shear stress only yields

$$\tilde{\sigma}_{11}(\tilde{x}_1, 0^+) = \begin{cases} B_T(\tilde{x}_1^2 - 1)^{e_T} + O(1), & e_T \in (-1, 0) \\ B_T \ln(\tilde{x}_1^2 - 1) + O(1), & e_T = 0 \end{cases} \tag{57}$$

where B_T is a constant related to the distribution of the shear stress. For $-1 < e_T < 0$, no constant that functions like the SIF is observed in the calculation. The asymptotic solution of displacement component, u_2, under a power-law shear stress only is obtained from Eq. (37) as

$$\tilde{u}_2(\tilde{x}_1, 0^+) = D_T(1 - \tilde{x}_2)^{1+e_T}, \quad e_T \in (-1, 0) \tag{58}$$

where $D_T = -(1 - 2\nu)/2(1 - \nu)(1 + e_T) < 0$. Note that there is no higher order terms in Eq. (58) in the neighborhood of (1, 0).

4.3 Criteria of Crack Initiation

4.3.1 Subproblem (1). From Eq. (52), it is known that when $\tilde{x}_1$ approaches 1^-, the displacement caused by shear stress, which is characterized by $-(1 - \tilde{x}_1)$, decreases more quickly than that caused by normal stress, which is characterized by $\sqrt{1 - \tilde{x}_1}$. As a result, the right-hand side of Eq. (48) remains unchanged for an additional uniform shear stress acting on the crack surfaces. More rigorously, utilizing Eq. (48) of the SERR and Eqs. (52) and (54), there is

$$\tilde{G} = \lim_{\varepsilon \to 0^+} \frac{2}{\varepsilon} \int_0^{\varepsilon} \frac{\tilde{p}}{\sqrt{2\tilde{r}}} \left[\tilde{p}\sqrt{2(\varepsilon - \tilde{r})} + \frac{(1 - 2\nu)\tilde{\tau}}{2(1 - \nu)}(\varepsilon - \tilde{r}) \right] d\tilde{r} = \pi\tilde{p}^2 \tag{59}$$

where $\varepsilon = \Delta l/l$ is the dimensionless infinitesimal distance of the motion of crack tip and $\tilde{r}$ is the dimensionless distance from the crack tip. It is evident that a uniform symmetrical shear stress has no influence on the SERR. The equation of the SIF can be validated with Eq. (49), which yields

$$\tilde{K}_I = \lim_{\tilde{x}_1 \to 1} \sqrt{2} \left[\tilde{p} \left(\frac{\tilde{x}_1}{\sqrt{\tilde{x}_1^2 - 1}} - 1 \right) + \frac{2\tilde{\tau}}{\pi} \ln \frac{\tilde{x}_1^2}{\tilde{x}_1^2 - 1} \right] = \tilde{p} \tag{60}$$

The SIF that calculated from $\tilde{\sigma}_{11}$ is in accord with that calculated from $\tilde{\sigma}_{22}$ for uniform normal and shear stresses acting on the crack surfaces. A uniform shear stress leads to a logarithmic stress singularity at the crack tip, and its singularity is negligible compared to that due to normal stress such that $\tilde{K}_I$ is finite and positive. Thus, a uniform shear stress has no influence on the SIF.

4.3.2 Subproblem (2). Equations (55) and (57) are combined for $\tilde{\sigma}_{11}$, and Eqs. (56) and (58) are combined for $\tilde{u}_2$, with $e_P = 0$ and $e_T = -1/2$. From Eq. (48), the SERR is calculated as

$$\begin{aligned} \tilde{G} &= \lim_{\varepsilon \to 0^+} \frac{2}{\varepsilon} \int_0^{\varepsilon} \left[A_P(2\tilde{r})^{-1/2} + B_P \ln(2\tilde{r}) \right] \\ &\quad \times \left[\sqrt{2}C_P(\varepsilon - \tilde{r})^{1/2} + 2D_P(\varepsilon - \tilde{r}) + D_T(\varepsilon - \tilde{r})^{1/2} \right] d\tilde{r} \\ &= \frac{\pi}{\sqrt{2}} A_P(\sqrt{2}C_P + D_T) = \frac{\pi}{\sqrt{2}} \left(\sqrt{2} - \frac{1 - 2\nu}{1 - \nu} \right) > 0 \end{aligned} \tag{61}$$

Considering $A_P > 0$, the sign of $\tilde{G}$ is determined by C_P and D_T. In a problem with a large fracture toughness, C_P is likely much larger than D_T resulting in a positive $\tilde{G}$. Using Eqs. (49), (55), and (57), the SIF is given by

$$\begin{aligned} \tilde{K}_I &= \lim_{\tilde{x}_1 \to 1} \sqrt{2(\tilde{x}_1 - 1)} [A_P(\tilde{x}_1^2 - 1)^{-1/2} \\ &\quad + B_P \ln(\tilde{x}_1^2 - 1) + B_T(\tilde{x}_1^2 - 1)^{-1/2}] \\ &= A_P + B_T = 1 + B_T \end{aligned} \tag{62}$$

which is inconsistent with $\tilde{K}_I = \lim_{x_1 \to l^+} \sqrt{2(\tilde{x}_1 - 1)}\tilde{\sigma}_{22} = 1$. This inconsistency is due to the negative constant B_T that is from the singular shear stress. The leading term of $\tilde{\sigma}_{11}$ consists of the contributions of the normal and shear stresses. The sign of $\tilde{K}_I$ is determined by both $A_P = \lim_{x_1 \to l^+} \sqrt{2(\tilde{x}_1 - 1)}\tilde{\sigma}_{22}$ and B_T. The condition of $\tilde{K}_I$ being influenced by the shear stress is $e_T > -1/2$. Either the method of the SERR or the SIF breaks down. Considering the fundamental role of the SERR in fracture mechanics, the use of the SIF is inappropriate in subproblem (2).

4.3.3 Subproblem (3). The SERR is calculated using Eqs. (48) and (55)–(58) with $e_P = -1/3$ and $e_T = -2/3$ as

$$\tilde{G}=\lim_{\varepsilon\to 0^+}\frac{2}{\varepsilon}\int_0^{\varepsilon}\left[B_{\mathrm{P}}D_{\mathrm{P}}[2\tilde{r}(\varepsilon-\tilde{r})]^{1/3}+2^{-1/3}B_{\mathrm{P}}D_{\mathrm{T}}\tilde{r}^{-1/3}(\varepsilon-\tilde{r})^{1/3}\right]\mathrm{d}\tilde{r}$$
$$=\frac{2^{5/3}\pi B_{\mathrm{P}}D_{\mathrm{T}}}{3^{3/2}}<0 \tag{63}$$

It is evident that the SERR is negative and finite, and this situation is due to the combined effect of the singular normal and shear stresses. Either a smaller e_{P} or e_{T} will lead to a negative and singular $\tilde{G}$. The criterion of $\tilde{G}$ being singular is $e_{\mathrm{P}}+e_{\mathrm{T}}<-1$ for crack problems with $\lim_{\tilde{x}_1\to 1}\sqrt{2(\tilde{x}_1-1)}\tilde{\sigma}_{22}=0$. The SIF

$$\tilde{K}_{\mathrm{I}}=\lim_{\tilde{x}_1\to 1}\sqrt{2(\tilde{x}_1-1)}\left[B_{\mathrm{P}}\left(\tilde{x}_1^2-1\right)^{-1/3}+B_{\mathrm{T}}\left(\tilde{x}_1^2-1\right)^{-2/3}\right]$$
$$=\lim_{\tilde{x}_1\to 1}\frac{B_{\mathrm{T}}}{2^{1/6}(\tilde{x}_1-1)^{1/6}}\to-\infty \tag{64}$$

is negative and singular because of the shear stress, even though the normal stress has no contribution to $\tilde{K}_{\mathrm{I}}$. The criterion of $\tilde{K}_{\mathrm{I}}$ being singular is either $e_{\mathrm{P}}<-1/2$ or $e_{\mathrm{T}}<-1/2$.

The SERR, G, and the SIF, K_{I}, have long been used for constructing the crack initiation criteria [6,7,19]. The applicability of K_{I} is based on the inverse-square-root asymptotic solution of stress field and square-root asymptotic solution of displacement field. For normal-stress-only problems, these asymptotic solutions are guaranteed by an integral

$$\int_0^1\frac{\tilde{p}(\tilde{s})\mathrm{d}\tilde{s}}{\sqrt{1-\tilde{s}^2}} \tag{65}$$

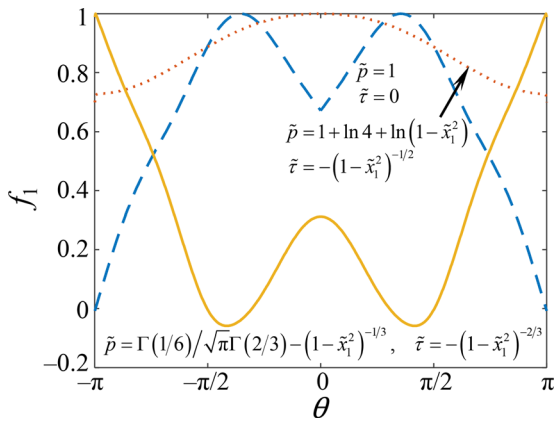

Fig. 6 Angular distributions of normalized maximum principal stress near the crack tip ($\tilde{r}=10^4$)

However, in subproblems (2) and (3), the asymptotic solutions consist of normal-stress and shear-stress parts. In subproblem (2), the leading terms of the two parts are of the same order and opposite signs. This results in the competition between the two parts. A higher value of e_{P} leads to higher value of the power-law exponents of displacement and stress fields. If the part of shear stress is larger than that of the normal stress, K_{I} is negative. If the crack continues to fracture, this correlation breaks down the applicability of K_{I}. And the subproblem (3) shows K_{I} being more sensitive to the singularity of shear stress than G. In subproblems (2) and (3), there is positive correlation between the power-law exponents of displacement and stress fields and e_{T}. The power-law exponents of displacement and stress

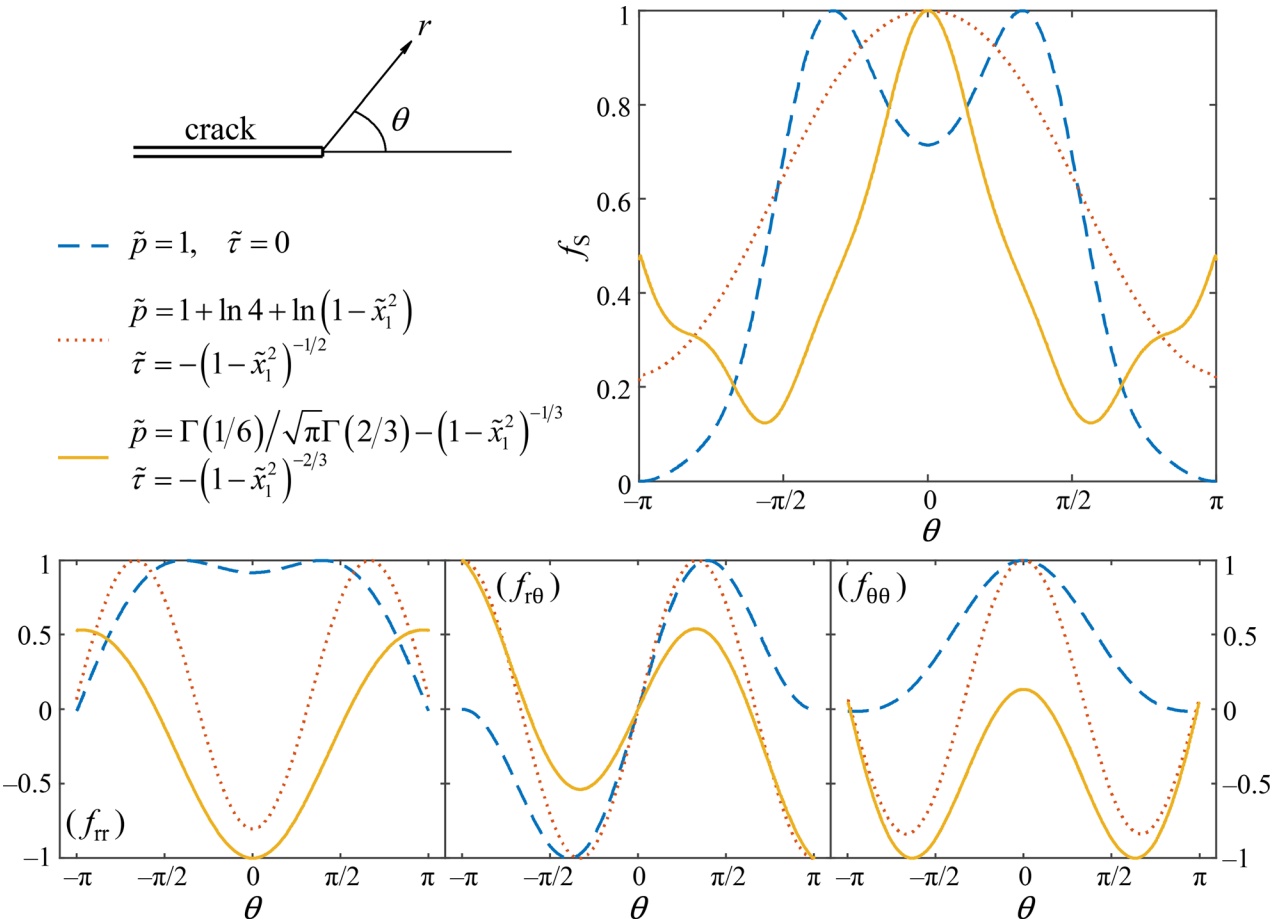

Fig. 5 Angular distributions of normalized strain energy density, f_{S}, and stress components, f_{rr}, $f_{r\theta}$ and $f_{\theta\theta}$, near the crack tip ($\tilde{r}=10^4$)

fields are smaller than that induced by normal stress, even smaller than 1/2 and −1/2, respectively, in subproblem (3). As a result, G and K_I are dominated by shear stress. Negative G and singular K_I emerge. When zero-K_I assumption is adopted, the critical value of the SERR approaches 0^+. However, in subproblem (3), G is negative definitely, and a negative G results in crack arrest. If the crack grows as assumed, both the crack initiation criteria break down.

4.4 Prediction of Crack Deflection. The angle of largest circumferential stress, $\sigma_{\theta\theta}$, maximum principal stress, σ_1, and strain energy density [9], S, have been used to predict the angle of crack deflection. Figure 5 plots the angular distributions of normalized strain energy density, f_S, and stress components, f_{rr}, $f_{r\theta}$ and $f_{\theta\theta}$, with $\tilde{r} = 10^{-4}$. As shown in the figure, θ and r are the coordinates of polar coordinate system with its origin being located at the crack tip.

For subproblem (1), these methods result in different solutions when subjected to the same load. The maximum value of circumferential stress exists in front of the crack tip, the maxima of S exist at two certain angles related to the Poisson's ratio, and σ_1 predicts two angles, which are slightly larger than that predicted by strain energy density, see Fig. 6. The crack will be fractured straightly or in a zigzag path, although the last two methods predict nonzero deflection angles. This is due to the redistribution of stress field after a crack deflection [21]. For subproblem (2), the three methods predict a same result as $\theta = 0$, i.e., the crack is fractured straightly and steadily. For subproblem (3), it is not easy to implement the largest circumferential stress method, because $f_{\theta\theta}$ is nearly negative anywhere around the crack tip except for 0 at $\theta = 0$ and $\pm\pi$, where $f_{\theta\theta}$ approaches 0^+ for $\tilde{r} \to 0$. As a result, the crack may keep propagating directly, or there may be subcracks developing from the crack surfaces. The maxima of S locate in front of the crack tip. However, this is due to $\tilde{\sigma}_{11}$, which is negative. If the crack keeps fracturing straightly, the released energy is mainly from the compressive stress other than the tensile stress. The second largest values of strain energy density locate near the crack surfaces, where f_{rr} has a largest positive value. If the crack fractures on the crack surface, tensile subcracks emerge from the crack surfaces behind the crack tip. According to Fig. 6, maximum principal stress gives plausible results as $\theta = \pm\pi$, which also suggest the developing of subcracks from the crack surfaces. However, as the stress field has singularity at the crack tip, the concept of principal stress needs to be validated for the problems with symmetrical loads. It still requires further investigations to demonstrate the applicability of the method of maximum principal stress.

4.5 Brief Discussion. Singular symmetrical shear stress may lead to the breakdown of the calculation of the SIF and the SERR. The breakdown may origin from (1) the inappropriate use of the theory of LEFM for hydraulic fracturing problems, (2) the one-way coupling of shear stress, and (3) the lack of generality of the model of hydraulic fracturing with combined effect of normal and shear stresses. For the first reason, there may exist a process zone around the crack tip. However, the solutions inside and outside the process zone should match each other at the boundary of process zone. The LEFM is proved to give a compressive circumferential stress around the crack tip for subproblem (3). The process zone is likely in compressive state in circumferential direction. Process zone results in a finite and negative SERR. The crack will be arrested, which is inconsistent with the assumption that the crack propagates straightly and continuously. Thus, the first reason may be, therefore, irrational. For the second reason, the influence of this one-way coupling is negligible for subproblem (2) [4]. For subproblem (3), real-time simulations are required to deal with the full coupling problem. While for the third reason, considering the results of Sec. 4.4, the assumption that the crack is fractured straightly and steadily may not be appropriate, or the fluid-lag zone behind the crack tip may not be negligible. There may be divergent or mesh-dependent results in numerical calculations. Effective and robust real-time numerical simulations with fluid lags are required to further investigate the fluid–solid process.

5 Conclusions

The quasi-static crack growth with symmetrical loads, including the normal and shear stresses, is studied. The theory of LEFM is used to describe the deformation and fracture behavior of a brittle solid. The solid is in the plane-strain state. By using the integral-transform method, the boundary integral equations of displacement and stress fields are derived for the full space. The analytical solution to a problem under the uniform normal and shear stresses is obtained. The analytical solution shows that a negative shear stress acting on the upper crack surface tends to inhibit the crack. The asymptotic solution near the crack tip of the displacement and stress fields is obtained under power-law normal and shear stresses. Due to the effect of shear stress, σ_{11} is suggested rather than σ_{22} to calculate the SIF. Three subproblems from hydraulic fracturing are discussed. The results reveal that

(1) singular symmetrical loads may lead to singular SIFs and SERRs, and the criterion of the SIF is inappropriate for either the fracture toughness or the fluid viscosity being extremely large;
(2) for the fracture toughness being extremely large, the largest values of circumferential stress, maximum principal stress, and strain energy density locate at $\theta = 0$, the crack is fractured straightly and steadily;
(3) for the fluid viscosity being extremely large, circumferential stress is largest at $\theta = 0$ and $\pm\pi$. A straight crack is told by the strain energy density. Crack branches on the crack surfaces behind the crack tip according to the maximum principal stress.

In hydraulic fracturing, the breakdowns of the criterion of crack initiation and the prediction of the crack deflection motivate future work on real-time numerical simulations incorporating shear stress and a fluid lag.

Acknowledgment

This research is supported in part by the National Natural Science Foundation of China (NSFC, Grant No. U1562105 and 11372313), and by the Chinese Academy of Sciences (CAS) through CAS Interdisciplinary Innovation Team Project, the CAS Key Research Program of Frontier Sciences (Grant No. QYZDJ-SSW-JSC019) and the CAS Strategic Priority Research Program (Grant No. XDB22040401).

Funding Data

- Chinese Academy of Sciences (QYZDJ-SSW-JSC019)
- National Natural Science Foundation of China (U1562105)

Nomenclature

$A(x_1, k), B(x_1, k)$ = unknown functions after the Fourier transformation
E, E' = Young's modulus, $E' = E/(1-\nu^2)$
$f_{rr}, f_{r\theta}, f_{\theta\theta}$ = normalized stress components
f_1, f_S = normalized maximum principal stress and strain energy density
$\mathcal{F}_s, \mathcal{F}_c$ = Fourier sine and cosine transforms
$\mathcal{F}_s^{-1}, \mathcal{F}_c^{-1}$ = inverse Fourier sine and cosine transforms
G = energy release rate
$I_P(x_1, x_2)$ = iterated integral of the normal stress
$I_T(x_1, x_2)$ = iterated integral of the shear stress
$J_0(*)$ = Bessel function of the first kind
k = Fourier transform of x_1
K_I = stress intensity factor of a mode I crack
l = crack length
LEFM = linear elastic fracture mechanics
$p(x_1)$ = the distribution of negative normal stress acting on the crack surfaces
S = strain energy density

s, t = lengths, variables in finite integrals
SERR = strain energy release rate
SIF = stress intensity factor
$\boldsymbol{u}, u_1, u_2$ = displacement vector and its components
$\boldsymbol{U}, U_1, U_2$ = Fourier transforms of the displacement vector and its components
$Z_{P,k}(x_1, x_2)$ = single integral of the normal stress
$Z_{T,k}(x_1, x_2)$ = single integral of the shear stress
$\boldsymbol{\gamma}, \gamma$ = strain tensor and its trace
$\Gamma(*)$ = Gamma function
λ, μ = Lamé constants
ν = Poisson's ratio
Ξ = Fourier transform of the trace of strain tensor
σ_1 = maximum principal stress
$\sigma_{\theta\theta}$ = circumferential stress around the crack tip
$\boldsymbol{\sigma}, \sigma_{11}, \sigma_{12}, \sigma_{22}$ = stress tensor and its components
$\tau(x_1)$ = distribution of shear stress acting on the crack surfaces
$\varphi(t), \psi(t)$ = auxiliary functions of preliminary results
The $\sim$ above a variable represents that the variable is dimensionless

Appendix A: Derivation of the Auxiliary Variables $\varphi(t)$ and $\psi(t)$

Using the characteristics of sine and cosine functions, Eqs. (16), (18), and (19) are rewritten as

$$\frac{\mathrm{d}}{\mathrm{d}x}\mathcal{F}_{\mathrm{s}}^{-1}\left\{\frac{A}{k}+2B\right\}=\frac{\Delta p(x_1)}{\mu},\quad \text{for } x_1\in(0,l) \tag{A1}$$

$$\frac{\mathrm{d}}{\mathrm{d}x}\mathcal{F}_{\mathrm{c}}^{-1}\left\{\frac{1-\nu}{(1-2\nu)k}A+B\right\}=\frac{\tau(x_1)}{2\mu},\quad \text{for } x_1\in(0,l) \tag{A2}$$

$$\frac{\mathrm{d}}{\mathrm{d}x}\mathcal{F}_{\mathrm{c}}^{-1}\left\{\frac{1-\nu}{(1-2\nu)k}A+B\right\}=0,\quad \text{for } x_1\in(l,\infty) \tag{A3}$$

Substituting Eq. (20) into Eq. (A2), one obtains

$$\sqrt{\frac{2}{\pi}}\frac{\mathrm{d}}{\mathrm{d}x}\int_0^l\psi(t)\mathrm{d}t\int_0^\infty J_0(kt)\cos(kx_1)\mathrm{d}k=-\frac{\tau(x_1)}{2\mu} \tag{A4}$$

with which Eq. (21) can be reduced to

$$\sqrt{\frac{2}{\pi}}\frac{\mathrm{d}}{\mathrm{d}x}\int_x^l\frac{\psi(t)\mathrm{d}\zeta}{\sqrt{t^2-x^2}}=\frac{\tau(x_1)}{2\mu} \tag{A5}$$

Using the solution of Abel integral equations [18], i.e.,

$$\begin{cases} f(t)=\displaystyle\int_0^t\frac{g(x)\mathrm{d}x}{\sqrt{t^2-x^2}} \\ g(x)=\displaystyle\frac{2}{\pi}\frac{\mathrm{d}}{\mathrm{d}x}\int_0^x\frac{tf(t)\mathrm{d}t}{\sqrt{x^2-t^2}} \end{cases} \quad \text{and} \quad \begin{cases} f(t)=\displaystyle\int_t^l\frac{g(x)\mathrm{d}x}{\sqrt{x^2-t^2}} \\ g(x)=\displaystyle-\frac{2}{\pi}\frac{\mathrm{d}}{\mathrm{d}x}\int_x^l\frac{tf(t)\mathrm{d}t}{\sqrt{t^2-x^2}} \end{cases} \tag{A6}$$

the solution of Eq. (A5) is found as

$$\psi(t)=-\sqrt{\frac{2}{\pi}}\frac{t}{2\mu}\int_t^l\frac{\tau(x_1)\mathrm{d}x_1}{\sqrt{x_1^2-t^2}} \tag{A7}$$

Using Eq. (20), one has

$$\frac{A}{k}+2B=\frac{1-2\nu}{1-\nu}\int_0^l\psi(t)J_0(kt)\mathrm{d}t+\frac{1}{1-\nu}\int_0^l\varphi(t)J_0(kt)\mathrm{d}t \tag{A8}$$

Similarly, $\varphi(t)$ can be expressed as

$$\varphi(t)=\frac{(1-\nu)t}{\mu}\sqrt{\frac{2}{\pi}}\int_0^t\frac{\Delta p(s)\mathrm{d}s}{\sqrt{t^2-s^2}}+\frac{(1-2\nu)t}{2\mu}\sqrt{\frac{2}{\pi}}\int_t^l\frac{\tau(s)\mathrm{d}s}{\sqrt{s^2-t^2}} \tag{A9}$$

Appendix B: Derivation of Boundary Integral Equations With I_{P} and I_{T}

The derivations of boundary integral equations for each component of displacement and stress are similar. In this Appendix, only the detail of u_1 is provided. Substituting the solutions of auxiliary functions (22) and (23) into Eq. (14), and there is

$$\begin{aligned} u_1(x_1,x_2)=&-\frac{2(1-\nu)}{\pi\mu}\int_0^l t\mathrm{d}t\left[\frac{1-2\nu}{2(1-\nu)}\int_0^t\frac{p(s)\mathrm{d}s}{\sqrt{t^2-s^2}}+\int_t^l\frac{\tau(s)\mathrm{d}s}{\sqrt{s^2-t^2}}\right]\\ &\times\int_0^\infty J_0(kt)\mathrm{e}^{-kx_2}\sin(kx_1)\mathrm{d}k\\ &+\frac{x_2}{\pi\mu}\int_0^l t\mathrm{d}t\left[\int_0^t\frac{p(s)\mathrm{d}s}{\sqrt{t^2-s^2}}+\int_t^l\frac{\tau(s)\mathrm{d}s}{\sqrt{s^2-t^2}}\right]\\ &\times\int_0^\infty kJ_0(kt)\mathrm{e}^{-kx_2}\sin(kx_1)\mathrm{d}k \end{aligned} \tag{B1}$$

The second term on the right-hand side can be reduced with $\partial\cos(kx_1)/\partial x_1=-k\sin(kx_1)$ such that

$$\begin{aligned} u_1(x_1,x_2)=&-\frac{2(1-\nu)}{\pi\mu}\int_0^l t\mathrm{d}t\left[\frac{1-2\nu}{2(1-\nu)}\int_0^t\frac{p(s)\mathrm{d}s}{\sqrt{t^2-s^2}}+\int_t^l\frac{\tau(s)\mathrm{d}s}{\sqrt{s^2-t^2}}\right]\\ &\times\int_0^\infty J_0(kt)\mathrm{e}^{-kx_2}\sin(kx_1)\mathrm{d}k\\ &-\frac{x_2}{\pi\mu}\frac{\partial}{\partial x_1}\int_0^l t\mathrm{d}t\left[\int_0^t\frac{p(s)\mathrm{d}s}{\sqrt{t^2-s^2}}+\int_t^l\frac{\tau(s)\mathrm{d}s}{\sqrt{s^2-t^2}}\right]\\ &\times\int_0^\infty J_0(kt)\mathrm{e}^{-kx_2}\cos(kx_1)\mathrm{d}k \end{aligned} \tag{B2}$$

The infinite integral of Bessel function, exponential function, and trigonometric function can be simplified by Euler equation, $\mathrm{e}^{-\mathrm{i}kx_1}=\cos(kx_1)+\mathrm{i}\sin(kx_1)$. According to Ref. [22], there is

$$\begin{aligned} &\int_0^\infty J_0(kt)\mathrm{e}^{-kx_2}\cos(kx_1)\mathrm{d}k+\mathrm{i}\int_0^\infty J_0(kt)\mathrm{e}^{-kx_2}\sin(kx_1)\mathrm{d}k\\ &=\frac{1}{\sqrt{(x_2-\mathrm{i}x_1)^2+t^2}} \end{aligned} \tag{B3}$$

Substituting Eq. (B3) into Eq. (B2), the displacement component, u_1, is

$$\begin{aligned} u_1(x_1,x_2)=&-\frac{2(1-\nu)}{\pi\mu}\int_0^l t\mathrm{d}t\left[\frac{1-2\nu}{2(1-\nu)}\int_0^t\frac{p(s)\mathrm{d}s}{\sqrt{t^2-s^2}}+\int_t^l\frac{\tau(s)\mathrm{d}s}{\sqrt{s^2-t^2}}\right]\\ &\times\mathrm{Im}\frac{1}{\sqrt{(x_2-\mathrm{i}x_1)^2+t^2}}\\ &-\frac{x_2}{\pi\mu}\frac{\partial}{\partial x_1}\int_0^l t\mathrm{d}t\left[\int_0^t\frac{p(s)\mathrm{d}s}{\sqrt{t^2-s^2}}+\int_t^l\frac{\tau(s)\mathrm{d}s}{\sqrt{s^2-t^2}}\right]\\ &\times\mathrm{Re}\frac{1}{\sqrt{(x_2-\mathrm{i}x_1)^2+t^2}} \end{aligned} \tag{B4}$$

With the definition of I_{P} and I_{T} and $\mu=(1-\nu)E'/2$, u_1 is expressed as

$$u_1(x_1,x_2) = -\frac{4}{\pi E'}\mathrm{Im}\left[\frac{1-2\nu}{2(1-\nu)}I_\mathrm{P} + I_\mathrm{T}\right] - \frac{2x_2}{\pi E'(1-\nu)}\frac{\partial}{\partial x_1}\mathrm{Re}(I_\mathrm{P}+I_\mathrm{T}) \tag{B5}$$

Appendix C: Displacement and Stress Fields in Full Space

Due to the symmetry, the components of displacement and shear stress in full space can be expressed with that in the first quadrant as

$$\begin{aligned}(u_1,u_2,\sigma_{11},\sigma_{12},\sigma_{22})(x_1,x_2) &= (-u_1,u_2,\sigma_{11},-\sigma_{12},\sigma_{22})(-x_1,x_2)\\ &= (-u_1,-u_2,\sigma_{11},\sigma_{12},\sigma_{22})(-x_1,-x_2)\\ &= (u_1,-u_2,\sigma_{11},-\sigma_{12},\sigma_{22})(x_1,-x_2)\end{aligned} \tag{C1}$$

The following derivation focuses on the first quadrant where $x_1 \geq 0$ and $x_2 \geq 0$. There is difficulty in directly integrating Eqs. (24), (25), and (38)–(40) because of the complexity of I_T. Thus, a hybrid approach of I_P and $Z_{\mathrm{T},0}$ is used. I_P is used for normal stress and $Z_{\mathrm{T},0}$ is used for shear stress. The derivatives of I_P and $Z_{\mathrm{T},0}$ are

$$\frac{\partial I_\mathrm{P}}{\partial \tilde{x}_1} = \frac{\mathrm{i}\pi\tilde{p}}{2}\left[1 - 1\Big/\sqrt{1+\frac{1}{(\tilde{x}_2-\mathrm{i}\tilde{x}_1)^2}}\right] \tag{C2}$$

$$\frac{\partial^2 I_\mathrm{P}}{\partial \tilde{x}_1^2} = -\mathrm{i}\pi\tilde{p}/2\left[1-(\tilde{x}_1+\mathrm{i}\tilde{x}_2)^2\right]\sqrt{1+(\tilde{x}_1+\mathrm{i}\tilde{x}_2)^2} \tag{C3}$$

$$Z_{\mathrm{T},1} = \frac{\mathrm{i}\tilde{\tau}}{2}\ln\left[1+\frac{1}{(\tilde{x}_2-\mathrm{i}\tilde{x}_1)^2}\right] \tag{C4}$$

$$Z_{\mathrm{T},2} = -\frac{\tilde{\tau}}{(\tilde{x}_2-\mathrm{i}\tilde{x}_1)\left[1+(\tilde{x}_2-\mathrm{i}\tilde{x}_1)^2\right]} \tag{C5}$$

Note that the points (0, 0) and (0, 1) are not included because of the singularities. At point (0, 0), there are

$$\tilde{u}_1 = 0, \quad \tilde{u}_2 = \tilde{p} + \frac{1-2\nu}{2(1-\nu)}\tilde{\tau}, \quad \tilde{\sigma}_{11} = \infty, \quad \tilde{\sigma}_{12} = \tilde{\tau} \ \text{ and } \ \tilde{\sigma}_{22} = -\tilde{p} \tag{C6}$$

And at point (0, 1), there are

$$\tilde{u}_1 = -\frac{1-2\nu}{2(1-\nu)}\tilde{p} - \frac{2\ln 2}{\pi}\tilde{\tau}, \ \tilde{u}_2 = 0, \ \tilde{\sigma}_{11} = \infty, \quad \tilde{\sigma}_{12} = 0 \ \text{ and } \ \tilde{\sigma}_{22} = \infty \tag{C7}$$

References

[1] Spence, D. A., and Sharp, P., 1985, "Self-Similar Solutions for Elastohydrodynamic Cavity Flow," Proc. R. Soc. London, Ser. A, **400**(1819), pp. 289–313.
[2] Tsai, V. C., and Rice, J. R., 2010, "A Model for Turbulent Hydraulic Fracture and Application to Crack Propagation at Glacier Beds," J. Geophys. Res.: Earth Surf., **115**(F3), p. F03007.
[3] Detournay, E., 2016, "Mechanics of Hydraulic Fractures," Annu. Rev. Fluid Mech., **48**(1), pp. 311–339.
[4] Wrobel, M., Mishuris, G., and Piccolroaz, A., 2017, "Energy Release Rate in Hydraulic Fracture: Can We Neglect an Impact of the Hydraulically Induced Shear Stress?," Int. J. Eng. Sci., **111**, pp. 28–51.
[5] Yang, F. Q., and Zhao, Y. P., 2016, "The Effect of a Capillary Bridge on the Crack Opening of a Penny Crack," Soft Matter, **12**(5), pp. 1586–1592.
[6] Griffith, A. A., 1921, "The Phenomena of Rupture and Flow in Solids," Philos. Trans. R. Soc. London, Ser. A, **221**(582–593), pp. 163–198.
[7] Irwin, G. R., 1957, "Analysis of Stresses and Strains Near the End of a Crack Traversing a Plate," ASME J. Appl. Mech., **24**, pp. 361–364.
[8] Rice, J. R., 1968, "A Path Independent Integral and the Approximate Analysis of Strain Concentration by Notches and Cracks," ASME J. Appl. Mech., **35**(2), pp. 379–386.
[9] Sih, G. C., 1974, "Strain-Energy-Density Factor Applied to Mixed Mode Crack Problems," Int. J. Fract., **10**(3), pp. 305–321.
[10] Sneddon, I. N., and Lowengrub, M., 1969, *Crack Problems in the Classical Theory of Elasticity*, Wiley, New York.
[11] Williams, M. L., 1956, "On the Stress Distribution at the Base of a Stationary Crack," ASME J. Appl. Mech., **24**(1), pp. 109–114.
[12] Geertsma, J., and de Klerk, F., 1969, "A Rapid Method of Predicting Width and Extent of Hydraulically Induced Fractures," J. Pet. Technol., **21**(12), pp. 1571–1581.
[13] Desroches, J., Detournay, E., Lenoach, B., Papanastasiou, P., Pearson, J. R. A., Thiercelin, M., and Cheng, A., 1994, "The Crack Tip Region in Hydraulic Fracturing," Proc. R. Soc. London, Ser. A, **447**(1929), pp. 39–48.
[14] Jeffrey, R. G., 1989, "The Combined Effect of Fluid Lag and Fracture Toughness on Hydraulic Fracture Propagation," Low Permeability Reservoirs Symposium, Denver, CO, Mar. 6–8, SPE Paper No. SPE-18957-MS.
[15] Advani, S., Lee, T. S., Dean, R. H., Pak, C. K., and Avasthi, J. M., 1997, "Consequences of Fluid Lag in Three-Dimensional Hydraulic Fractures," Int. J. Numer. Anal. Methods Geomech., **21**(4), pp. 229–240.
[16] Garagash, D. I., 2006, "Propagation of a Plane-Strain Hydraulic Fracture With a Fluid Lag: Early-Time Solution," Int. J. Solids Struct., **43**(18), pp. 5811–5835.
[17] Yang, F., 1998, "Indentation of an Incompressible Elastic Film," Mech. Mater., **30**(4), pp. 275–286.
[18] Gorenflo, R., and Vessella, S., 1991, *Abel Integral Equations*, Springer Science & Business Media, Berlin.
[19] Lawn, B., 1993, *Fracture of Brittle Solids*, Cambridge University Press, Cambridge, UK.
[20] Zhao, Y. P., 2016, *Modern Continuum Mechanics* (in Chinese), Science Press, Beijing, China.
[21] Zhao, Y. P., 2014, *Nano and Mesoscopic Mechanics* (in Chinese), Science Press, Beijing, China.
[22] Jeffrey, A., and Daniel, Z., 2007, *Table of Integrals, Series, and Products*, Academic Press, Burlington, VT.